J Digit Imaging (2012) 25:580–590
DOI 10.1007/s10278-011-9450-6

# An Effective Approach of Lesion Segmentation Within the Breast Ultrasound Image Based on the Cellular Automata Principle

**Yan Liu · H. D. Cheng · Jianhua Huang · Yingtao Zhang · Xianglong Tang**

Published online: 12 January 2012


**Abstract** In this paper, a novel lesion segmentation within breast ultrasound (BUS) image based on the cellular automata principle is proposed. Its energy transition function is formulated based on global image information difference and local image information difference using different energy transfer strategies. First, an energy decrease strategy is used for modeling the spatial relation information of pixels. For modeling global image information difference, a seed information comparison function is developed using an energy preserve strategy. Then, a texture information comparison function is proposed for considering local image difference in different regions, which is helpful for handling blurry boundaries. Moreover, two neighborhood systems (von Neumann and Moore neighborhood systems) are integrated as the evolution environment, and a similarity-based criterion is used for suppressing noise and reducing computation complexity. The proposed method was applied to 205 clinical BUS images for studying its characteristic and functionality, and several overlapping area error metrics and statistical evaluation methods are utilized for evaluating its performance. The experimental results demonstrate that the proposed method can handle BUS images with blurry boundaries and low contrast well and can segment breast lesions accurately and effectively.

**Keywords** Breast neoplasm · Image segmentation · Ultrasound · Cellular automata

Y. Liu · H. D. Cheng · J. Huang · Y. Zhang · X. Tang
School of Computer Science and Technology,
Harbin Institute of Technology,
Harbin, No. 92, Xidazhi Street,
Harbin 150001, People's Republic of China

Y. Liu
College of Science, Harbin Institute of Technology,
Harbin, No. 92, Xidazhi Street,
Harbin 150001, People's Republic of China

H. D. Cheng (✉)
Department of Computer Science, Utah State University,
Logan, UT 84322, USA
e-mail: hengda.Cheng@usu.edu

## Introduction

Breast cancer is one of the most common cancers and affects women's health seriously [1]. Early detection is an effective way to control the disease [2]. Breast ultrasound (BUS) imaging has become one of the most prevalent and popular approaches for breast cancer diagnosis due to the fact that it is radiation-free, noninvasive, painless, cost-effective, and portable. However, the interpretation of BUS images depends on radiologists' skill and experience. In order to improve the effectiveness and accuracy, computer-aided diagnostic (CAD) techniques are more and more applied to clinical practice.

Lesion segmentation of a BUS image plays an important role in CAD systems. Its goal is to locate lesion regions to provide necessary information for feature extraction and classification [3]. Many methods based on different models for segmenting the breast lesions were published: histogram thresholding [4, 5], region growing [6, 7], Markov random fields [8–10], active contour model [11, 12], neural network [13, 14], cell competition [15], level set [16–18], etc. In most model-based methods, an energy function is formulated according to the initial condition and optimized to the local minimum. But if the initial condition is not right, the process may obtain poor results. Existing methods usually produce initial conditions by thresholding, clustering, region growing, etc. In blurred boundaries, the gray levels between neighboring pixels may be quite

similar. Without spatial information, normal tissues could be easily partitioned into lesion regions, and the produced initial conditions may be very poor (Fig. 1). In addition, the quality of ultrasound image is degraded by speckle noise. Although some speckle-removing methods were utilized for reducing noise [19, 20], the trade-off between noise suppression and feature preservation is a dilemma. Speckle patterns can reflect the local echogeneity of the underlying scatters, which can be employed by some methods, e.g., MRF-based methods [21], and the details of the images may be damaged after noise removal. Therefore, developing a method insensitive to initial condition and robust to noise is useful for solving a breast lesion segmentation task.

Cellular automata (CA) can produce highly complex patterns with relatively simple initial conditions and rules [22]. The concept of CA is to measure the differences between current cells and to evolute according to local rules operating on a given neighborhood [23]. Based on the CA priciple, several image preprocessing tasks including image denoising [24], edge detection [25], feature extraction [23], etc., were studied. The CA principle was also employed for image segmentation [26]. In this method, each pixel's state is iteratively updated according to the evolution rule: when the difference of neighboring pixels is larger, the energy decreases more greatly until the automaton converges to a stable configuration. However, only considering the relationship of neighboring pixels cannot deal with the characteristics (low SNR, blurry boundaries, heterogeneous gray levels, etc.) of BUS images well. Due to speckle noise, the energy may be transited unstably by the rapid change of gray levels and the automaton may converge in a wrong position (Fig. 2). In addition, previous works based on the CA framework only utilized the von Neumann or Moore neighboring system as the evolutive environment. If the von Neumann system is utilized, only a few pixels are considered and the cell automaton may converge prematurely. On the other hand, if more pixels are considered, as in the Moore system, the computational complexity could be very high, and it may not be useful for handing speckle noise. Thus, developing a new energy transfer strategy and environment for CA evolution is important and helpful for segmenting BUS images.

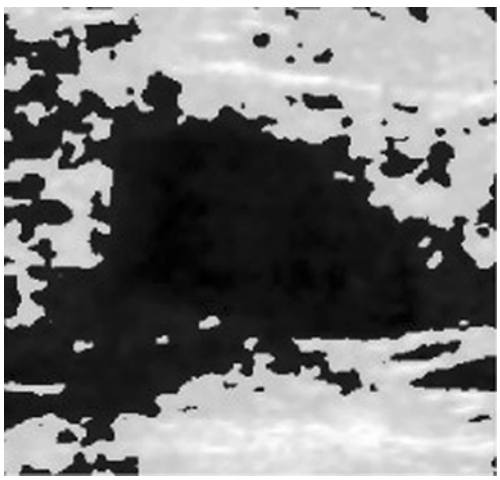

**Fig. 1** Pre-proceed image by thresholding

In this paper, a novel breast lesion segmentation approach utilizing the CA principle is proposed. In an energy transition function, the global and local information and the relationship between neighboring pixels can be integrated conveniently. Using different energy transfer strategies, the gray level distribution and spatial relation of the pixels can be calculated accordingly. For modeling global image information, a seed information comparison function is proposed by comparing the current pixel with the corresponding seed pixel. For detecting the corresponding seed pixels, an energy preserve strategy is developed and utilized. For modeling local image information difference, the gray level differences of neighboring pixels and the texture differences in the corresponding neighborhood system are calculated, which is helpful for processing the blurry boundaries. Moreover, an energy decrease strategy is used for modeling the spatial relation of pixels. Then, a similarity-based criterion is utilized in the Moore neighborhood system and mixed with the von Neumann neighborhood system as the evolution environment. By using the similarity-based criterion, speckle noise can be filtered without increasing the computation complexity much. The segmentation results demonstrate that the proposed approach can handle the blurry boundaries well, is insensitive to initial condition, and is also adaptive to noise effectively.

## Materials and Methods

### Image Acquisition

There were 205 BUS images (125 benign and 80 malignant) collected using HITACHI Vision 900 system (Hitachi Medical System, Tokyo, Japan) equipped with a liner probe whose central frequency is 6–13 MHz and captured directly from video signals. The images were obtained from the Second Affiliated Hospital of Harbin Medical University (Harbin, China). All patients were examined and diagnosed by an experienced radiologist according to image characteristics, including lesion shape, internal echo, capsule, attenuation, and blood flow, and the results were all confirmed by pathological examinations or biopsy. Informed consent to the protocol was approved by all patients. Manual delineations by an experienced radiologist are used as the gold standards because of the absence of more experts. According to [7, 17],

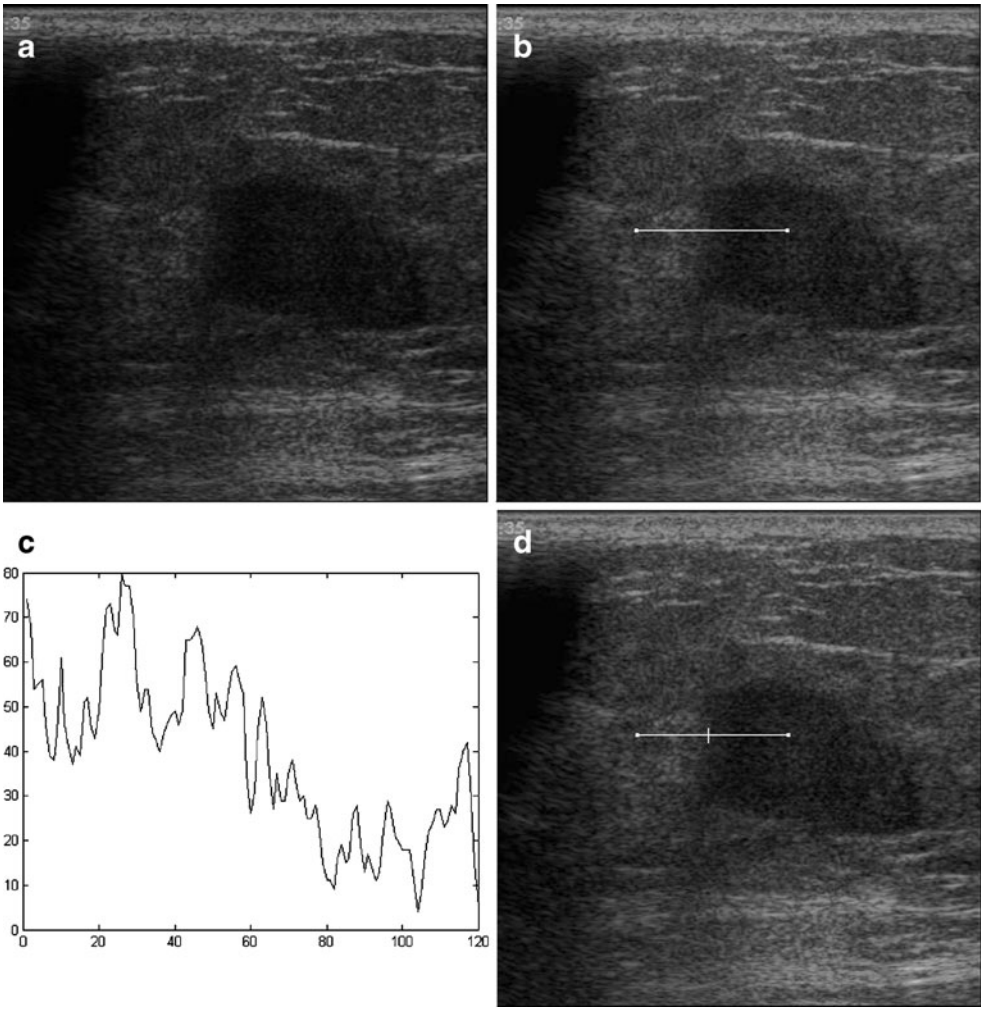


**Fig. 2** Convergent position of the grow cut approach. **a** Original BUS image. **b** Initial condition. **c** Corresponding intensities of the dashed line. **d** Segmentation result of the marked area by the grow cut method

the evaluation of segmentation performance by an expert is available.

## Overview of the Proposed Method

In this study, a 2D ultrasound image is considered as a cell space. At each time step, the cell state belongs to a finite set and is calculated according to the image information from a given neighborhood. The CA updates the entire lattice at discrete time and the change dynamics is determined by the energy transition function. With the evolution rule, if the features of two neighboring pixels are similar, the pixel with the weaker strength is very possible to be updated as the same label of the pixel with the stronger strength. With this rule, when the evolution converges, the unlabeled pixel will probably have the same label of the corresponding seed pixel if they have similar features. In addition, the neighboring pixels with similar features will also have the same label. The segmentation process is iterated until the automaton converges to a stable configuration. The block diagram is illustrated in Fig. 3.

## Initial Condition

To demonstrate that the proposed method is insenstive to the initial condition, we use a simple data set as the initial seed

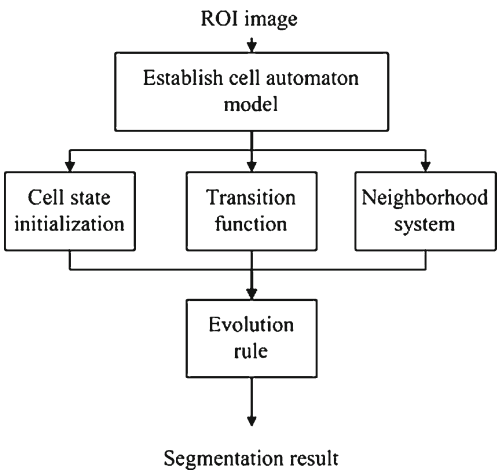


**Fig. 3** Block diagram of the proposed method

pixels. In this paper, the segmentation is conducted in a region of interest (ROI) produced by an experienced radiologist; each ROI is a rectangle containing the lesion in its center. For producing the seed data set, pixels on the ROI boundary are used as the seeds for background. In a ROI, the data set is generated as the foreground seed pixels automatically.

$$A=\left\{(x,y)\left|\begin{array}{l}\left|x-\frac{x_1+x_2}{2}\right|\le\alpha|x_1-x_2|, y=x\cdot\frac{\beta|y_1-y_2|}{\alpha|x_1-x_2|}\\ or\left|y-\frac{y_1+y_2}{2}\right|\le\beta|y_1-y_2|, x=y\cdot\frac{\alpha|x_1-x_2|}{\beta|y_1-y_2|}\end{array}\right.\right\} \tag{1}$$

where $(x_1, x_1)$ and $(x_2, y_2)$ represent the diagonal coordinates of the ROI and the center point of the ROI is $\left(\frac{x_1+x_2}{2}, \frac{y_1+y_2}{2}\right)$. Parameters α and $\beta$ are used to determine the size of the foreground seed area. The evolution of the proposed method is an energy spreading/decreasing process in both space and time. If the ROI is too large, the energy of background seeds may decrease greatly and make the evolution converge prematurely. By experiment, the ROI selected by the radiologist is larger than 1.5 times the mass size and smaller than 2 times the mass size.

A cellular automaton can be defined as a triplet, $A=(S, N, O)$, where $S$ is a non-empty state set, $N$ is the neighborhood system, and $O{:}S^N\rightarrow S$ is the local transition function which defines the cell state affected by its surrounding cells in the neighborhood [22]. Considering an ultrasound image as a cell space, $(S', N', O')$, $S'$ expresses the pixels' states, $N'$ is neighborhood system, and $O'$ is the energy transition function, respectively. The initial state of each unlabeled pixel is a triplet $(l_p, \theta_p, E_p)$ which is set to:

$$l_p=0, \theta_p=0, E_p=V_p \tag{2}$$

where $l_p$ is the label, $\theta_p\in[0.1]$ is the strength, and $\boldsymbol{E}_p$ is the feature vector (energy) of pixel $p$. In this paper, the feature vector $\boldsymbol{E}_p$ is defined by pixel $p$'s gray level $(V_p)$. For each seed pixel, $p_{\text{seed}}$, the initial state is:

$$l_{p_{seed}}=\left\{\begin{array}{l}1\ if\ p_{seed}\in\text{foreground}\\ 2\ \text{if}\ p_{seed}\in\text{background}\end{array}\right., \ \theta_{p_{seed}}=1, \mathrm{E}_{p_{seed}}=V_{p_{seed}} \tag{3}$$

where $V_{p_{seed}}$ is the gray level of $p_{\text{seed}}$, $l_{p_{seed}}$ is the corresponding label, and the strength $\theta_{p_{seed}}$ is set to 1, which cannot be changed by other pixels. The task of segmentation is to assign each unlabeled pixel with one of the two possible labels (1 or 2) by using the transition function.

## Evolution Rule

The cell automaton starts to spread from the seed pixels and tries to occupy the whole image. By using the transition function, the state of each pixel $p$ at time step $t$ is updated according to the state of pixel $q$ at time step $t-1$

$$\left(l_p^t, \theta_p^t\right)=\left\{\begin{array}{l}\left(l_q^{t-1}, \mathrm{TF}\cdot\theta_q^{t-1}\right)\text{if}\ TF\cdot\theta_q^{t-1}>\theta_p^{t-1}\\ \left(l_p^{t-1}, \theta_p^{t-1}\right)\text{if}\ TF\cdot\theta_q^{t-1}\le\theta_p^{t-1}\end{array}\right. \tag{4}$$

where TF is the energy transition function, which will be defined later. At every iterative step, each pixel is either a defender $p$ whose state is updated by attacking or an attacker $q$ which attacks other pixels in its neighborhood; if the attacker's strength $\left(\mathrm{TF}\cdot\theta_q^t\right)$ is greater than the defender's strength, the defending pixel is infected and its label and strength are updated. Due to local competition, the pixel with the strongest strength occupies the neighboring sites and gradually spreads over the image. Through the evolution rule, the label of each pixel as foreground or background can be specified. The calculation continues until none of the pixel's state is changed, the automaton converges to a stable configuration, and the segmentation is finished.

## Transition Function and Neighborhood System

### *Seed Information Comparison Function*

The weights of different regions can be determined by two aspects. The first one is the local image information. This weight can characterize a pair of neighboring pixels whether they should be in the same class. If two of the neighboring pixels are in the same class, their features should be quite close. The second one is the area difference weight (global image information). This prior knowledge is based on both gray level distribution and spatial relation between pixels and the areas. If two pixels' features (gray level, Euclidian distance, etc.) are closer but belong to different areas (object or background), they may have different labels. Without area difference weight, different regions with close gray level distributions are treated equally, and the pixels in blurry regions may not be segmented well.

In this paper, we proposed a seed information comparison function for modeling the global image information. Seed pixels can express the object and background information well [27]; with this property, each pixel's class can be calculated more suitably. To detect the corresponding seed pixel, an energy preserve strategy is utilized. The evolution started from a seed pixel $p(0)$ at $t=0$. After $n$ iterations, its energy is spread to a defending pixel $p(t)$ at $t=n$. Then, the seed information comparison function (SIF) is defined as:

$$\mathrm{SIF}=\left|\sum_{t=1}^{n}\left(E_{p_{(t-1)}}-E_{p_{(t)}}\right)\right| \tag{5}$$

where $E_{p_{(t)}}$ is the gray level of pixel $p(t)$. This function is based on the following idea: in an energy transition chain, each current pixel $P_{(t)}$ is a defender attacked by the attacker $p_{(t-1)}$ at time $t$, and it is also an attacker $p_{(t)}$ which attacks other pixels at $t$+1. In each iteration, the defender's gray level in a previous time step is preserved and subtracts the attacker's gray level in the current time step, and the similarity between $p_0$ and $p_{(t)}$ can be acquired (Fig. 4).

### *Texture Information Comparison Function*

In a blurry boundary, the gray levels of neighboring pixels are quite similar, but the local texture between their corresponding neighborhoods may be different. This property is helpful for categorizing the pixel's class more exactly. The correlation is one of the most useful statistics that describes the relationship between two sets of data. In this paper, a texture information comparison function is proposed by comparing the correlation texture information and autocorrelation texture information between different neighborhoods. The correlation texture information is defined as [28]:

$$\mathrm{COR}_{pq} = \left|\mu_p - \mu_q\right| + \sqrt{\left(E_p - \mu_q\right)^2} \tag{6}$$

where $\mu_p$ and $\mu_q$ are the local mean values of the eight neighbors of defender $p$ and attacker $q$, respectively. Autocorrelation texture is a powerful tool for describing the spatial organization of pixels. For describing autocorrelation texture information, a co-occurrence matrix is utilized. Each element of the co-occurrence $C(i,j|d',\theta')$ is defined as the joint probability of gray levels $i$ and $j$ separated by distance $d'$ and along direction $\theta'$ [29]. The autocorrelation texture, ACOR, is defined as:

$$\mathrm{ACOR} = (d',\theta') = \frac{\sum_{i,j}(i-\mu_x)\left(j-\mu_y\right)C(i,j|d',\theta')}{\sigma_x\sigma_y} \tag{7}$$

$$\mu_x = -\sum_i i \sum_j C(i,j|d',\theta') \tag{8}$$

$$\mu_y = -\sum_j j \sum_i (i,j|d',\theta') \tag{9}$$

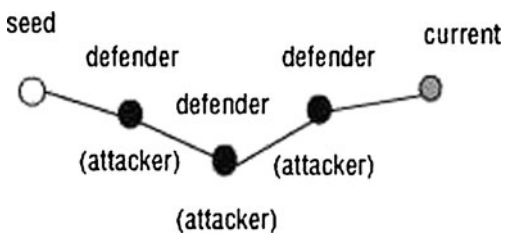


**Fig. 4** Energy transition chain of a seed pixel

$$\sigma_x = \sum_i (i-\mu_x)^2 \sum_j C(i,j|d',\theta') \tag{10}$$

$$\sigma_y = \sum_i (i-\mu_y)^2 \sum_j C(i,j|d',\theta') \tag{11}$$

where $x$, $y$ are the numbers of elements in the lattice. For each neighborhood of defender $p$ or attacker $q$, two kinds of texture are extracted and compared in the texture information comparison function, TIF.

$$\mathrm{TIF} = \mathrm{COR}_{pq} + \left|\mathrm{ACOR}_p - \mathrm{ACOR}_q\right| \tag{12}$$

Based on the above comparison function, the energy transition function, TF, is defined as:

$$\mathrm{TF} = \left(1 - \frac{\left|E_p - E_q\right| + \mathrm{TIF} + \mathrm{SIF}}{\kappa}\right) \tag{13}$$

where TF is a monotonously decreasing function and $\kappa$ is a constraint bounding TF to [0, 1]. For comparison, the values of $\left|E_p - E_q\right|$, TIF, SIF, and COR are normalized, respectively. Accordingly, the value of $\kappa$ is set to 4.

### *Neighborhood System Improvement*

Since the similarity of neighboring pixels can be calculated more exactly in a large scope of neighborhood system, Moore's neighborhood system is utilized for the evolution first.

$$N(p) = \left\{ q \in Z^d \,|\, \|p-q\|_\infty = \max_{i=1,d}|p_i - q_i| \le K \right\} \tag{14}$$

where $d$ is the number of elements in the neighborhood system and $K$ is the radius of Moore's neighborhood system. For handing speckle noise, a similarity-based criterion is utilized in Moore's neighborhood system as the following [30]:

$$\left|E_p - E_q\right| \le T \tag{15}$$

where $T$ is the threshold value. However, when a pixel is isolated, all its neighboring pixels may be filtered by the similarity-based criterion and the calculation may be wrong. To solve the problem, pixels in the von Neumann system are all considered. The von Neumann neighborhood is:

$$N(p) = \left\{ q \in Z^d \,|\, \|p-q\|_1 = \sum_{i=1}^{d} |p_i - q_i| = 1 \right\} \tag{16}$$

In the proposed method, the fixed area for determining the neighborhood is $S \times S$ pixels. In accordance with Eq. 15, when $K$ is 4, $S$=9.

Evaluation Methods

To evaluate the performance of segmentation, four error metrics—true-positive (TP) ratio, false-positive (FP) ratio, false-negative (FN) ratio, and similarity ratio (SI)—and a statistical evaluation with Hausdorff distance are utilized [18]. TP is expressed as the percentage of the real lesion area coverage. When the TP ratio is higher, more real lesion regions are classified as "breast lesion" regions. However, when both real lesion regions and normal tissues are classified as breast lesions, the TP ratio may be also quite high. In such cases, the error is made by FP. The FP ratio expresses the percentage of the normal tissues classified as the breast lesion regions. When the FP ratio is lower, fewer normal tissue regions are classified as breast lesion. The SI ratio expresses the similarity between the generated boundary and the radiologist's delineation. When it is higher, the segmentation result is more similar to the manual delineation and the overall performance is better. They are calculated as:

$$\mathrm{TP} = \frac{|A_\mathrm{m} \cap A_a|}{|A_m|}, FP = \frac{|A_m \cup A_\mathrm{a} - A_m|}{|A_m|}, \qquad (17)$$

$$\mathrm{FN} = \frac{|\mathrm{A_m} \cup \mathrm{A_a} - \mathrm{A_a}|}{|\mathrm{A_m}|}, \ \mathrm{SI} = \frac{|\mathrm{A_m} \cap \mathrm{A_a}|}{|\mathrm{A_m} \cup \mathrm{A_a}|}$$

where $A_\mathrm{a}$ is the pixel set determined by the algorithm and $A_\mathrm{m}$ is the pixel set determined by the radiologist manually. To validate the trade-off between the TP ratio versus the FP ratio, the receiver operator characteristic (ROC) curve is utilized for statistical analysis. Typically, the *TP* ratio is referred to as "sensitivity" and the FP ratio referred to as "specificity" [31]. The most commonly used global index of accuracy is the area under the ROC curve (AUC). An AUC close to 1.0 indicates that the segmentation has a higher accuracy.

Hausdorff distance is a classical statistical evaluation method that measures how far two subsets of a metric space are from each other. Define two boundary pixel sets of the lesion regions generated by different segmentation approaches as $A=\{a_1,a_2,\ldots,a_m\}$ and $B=\{b_1,b_2,\ldots,b_n\}$, where $a_u$ ($u=1\ldots m$) and $b_v$ ($v=1\ldots n$) are the coordinates of the pixels in sets $A$ and $B$, respectively. The Hausdorff distance is defined as:

$$H(A,B) = \max\{\max(h(A,B)), \max\{h(B,A)\}\} \qquad (18)$$

$$h(a_u,B) = \min_v \|a_u - b_v\|, \ h(b_v,A) = \min_u \|a_u - b_v\|$$

where $\|a_u - b_v\|$ is the Euclidean distance between pixels $a_u$ and $b_v$.

## Results

For studying the efficacy of the energy comparing function, the proposed method was applied to a BUS image first

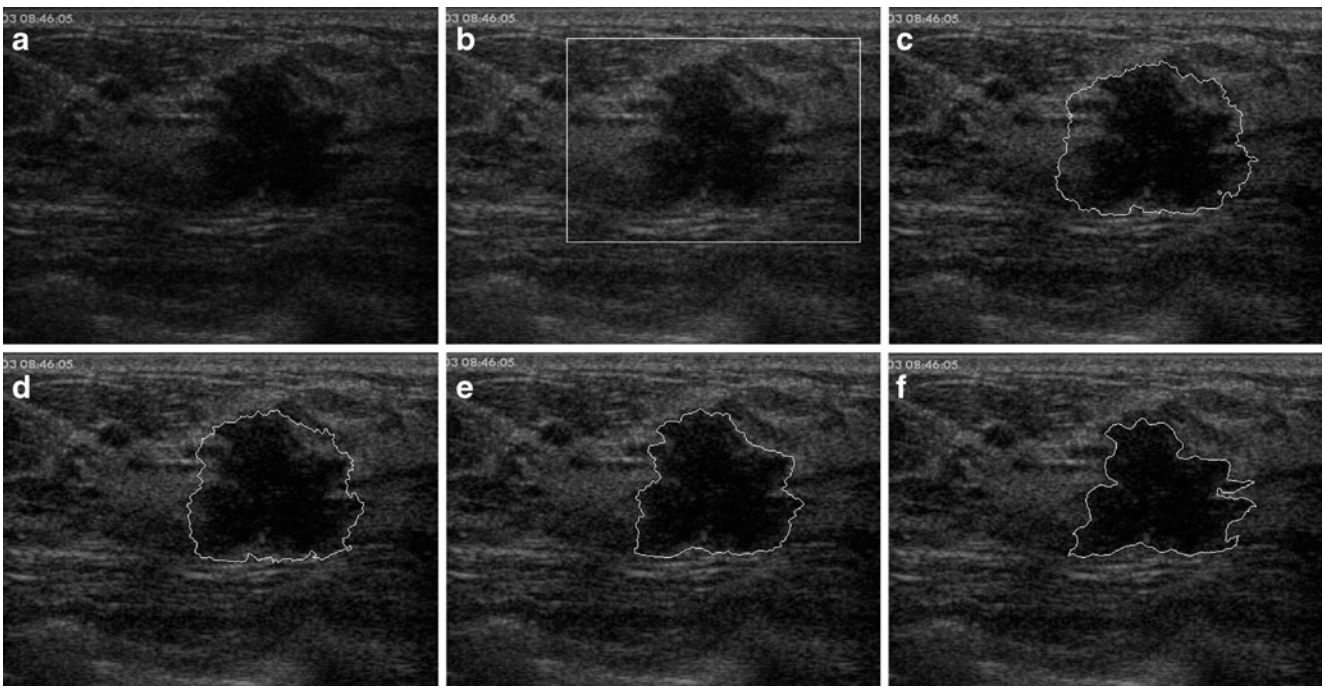


**Fig. 5** Segmentation result using different proposed energy comparing functions. **a** Original image with ROI delineated by the radiologist. **b** Initial condition. **c** Segmentation result only considering the gray level differences of neighboring pixels. **d** Segmentation result using a transition function with a texture comparison function. **e** Segmentation result using a transition function with a texture comparison function and a seed information comparison function. **f** Lesion region delineated by the radiologist

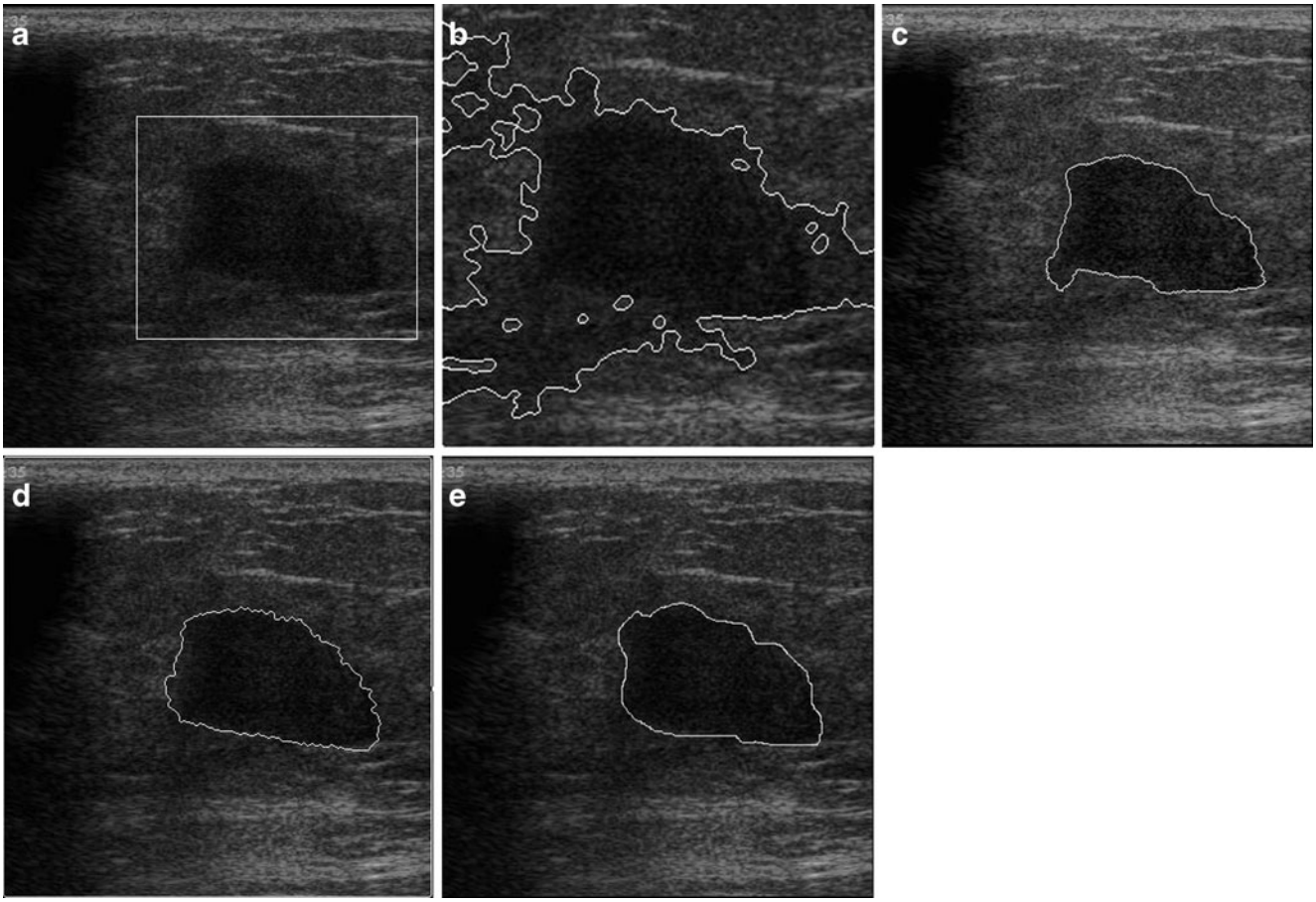


**Fig. 6** Segmentation result of an US image with high speckle noise. **a** Original image with marked ROI. **b** Segmentation result of the EBLS method. **c** Segmentation result of the LSAC method. **d** Segmentation result of the proposed method. **e** Lesion region delineated by the radiologist

(Fig. 5a). In some regions of the image, the contrast between the lesion and normal tissues is quite low. Figure 5c is the segmentation result generated by using the transition function formulated according to the difference of neighboring pixels. It is shown that the segmentation result does not converge at the position of the lesion boundary. Figure 5d is a lesion region segmented by employing the texture information comparison function. Compared with the lesion region delineated by the radiologist (Fig. 5f), fewer normal tissues are wrongly classified into the lesion region; it demonstrates that the proposed method can segment the breast lesion accurately.

The speckle noise is suppressed in two ways. The first is by using the seed information comparison function, where the strength of pixels can decrease more suitably; another way is that speckle noise can be suppressed by the similarity criterion. By adding the seed information comparison function, the segmentation result is generated in Fig. 5e. The segmentation result converges in a suitable position of the lesion region, and the generated boundary is much closer to the manual delineation. This demonstrates that using the proposed energy comparison function for segmentation is useful and effective.

The weights of $\alpha$ and $\beta$ are selected through experiments. In this study, $\alpha$=0.3 and $\beta$=0.3. The threshold value of the similarity criterion is $T = \sqrt{2}\sigma$, where $\sigma$ is the local standard deviation of the neighborhood.

To demonstrate the advantage of the proposed method in handling the speckle noise and blurry boundaries, two other recently published and prevalent model-based BUS image segmentation methods—edge-based level set (EBLS) model and level set-based active contour (LSAC) model—are also applied to the same images for comparison [16, 18]. The EBLS model has the following steps: (1) Speckle noise is suppressed by an anisotropic diffusion filter and stick filter [32, 33]. (2) The contrast of the image is enhanced by image thresholding, and the noise-suppressed image and the thresholded image are combined together to produce a preprocessed image. (3) Segmentation is done by an "edge-based" level set method. Furthermore, the level set method was utilized for segmenting the lesion of the processed image in step 2. The LSAC model is a level set-based active contour model whose energy function is formulated according to the differences between the estimated probability and the actual probability densities of the gray levels of different

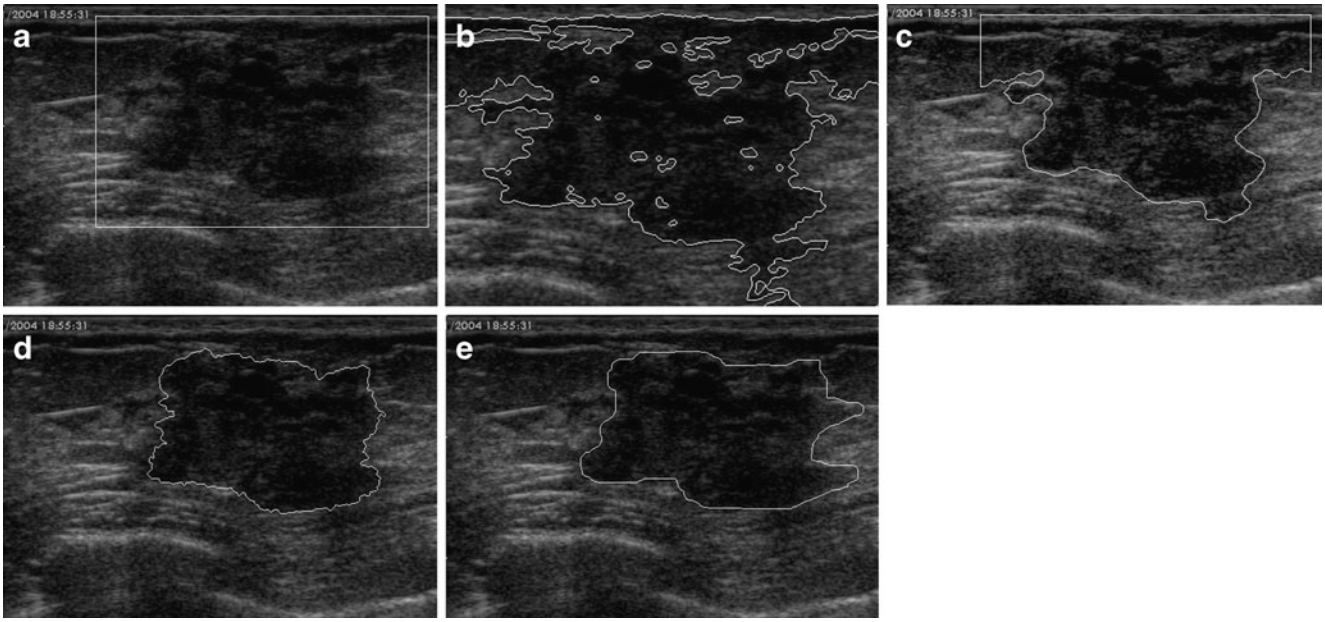


**Fig. 7** Segmentation of another BUS image with blurry boundaries. **a** Original image with marked ROI. **b** Segmentation result of the EBLS method. **c** Segmentation result of the LSAC method. **d** Segmentation result of the proposed method. **e** Lesion region delineated by the radiologist

regions. However, without utilizing spatial information, pixels with similar gray level distributions may not be processed well.

For comparison, three methods use the same initial condition for breast lesion segmentation and are applied to Fig. 6a first. It can be seen from Fig. 6b that the EBLS model cannot handle speckle noise well and did not converge on the real boundary of the lesion. By utilizing the proposed transition function, the proposed approach can handle noise very well, and the generated lesion region (Fig. 6d) is very close to the manual delineation (Fig. 6e). The result of the LSAC model is shown in Fig. 6c, which has a relatively good performance, but for the blurry boundaries, over-segmentation happens.

Figure 7a has a complicated structure, and the boundary of the lesion has multiply connected regions with the surrounding tissues. It is seen from the manual delineation (Fig. 7e) that the segmentation result by the EBLS model (Fig. 7b) was generated wrongly, and there were a lot of surrounding normal tissue regions included in the lesion region. This is because only the gray levels of different tissue regions are considered. In the thresholding step, the threshold value is defined by the mean value of each region. However, the mean value cannot describe the local features well. Since the "edge-based" level set method is sensitive to noise and the initial condition (Fig. 1), it may converge on an unsuitable local minimum. The same instance happened to the LSAC model, as shown in Fig. 7c.

From Fig. 7d, we can see that the proposed method can handle the blurry boundary well and that the generated lesion region is very close to the manual delineation. The proposed method produces better results for the following reasons: (1) The proposed method utilizes the global image information by using the seed information comparing function and the energy decrease strategy; the gray level distribution and the spatial relation of the pixels can be integrated effectively, which is useful for handling blurry boundaries. (2) Rather than considering the global texture information of the foreground/background simply, in the proposed method, the textures in every local region are fully considered. (3) Utilizing the improved neighborhood system, speckle noise can be handled well. (4) The proposed method utilizes the local image information directly by considering the relationship of neighboring pixels; therefore, the proposed method is insensitive to initial condition.

To evaluate the overall performance of different methods, the segmentation results of 205 images by employing the proposed method, the EBLS model, and the LSAC model were compared with those marked by the radiologist. The overlapping area error metrics of the three methods are shown in Table 1. From Table 1, it can be seen that the TP ratio of the EBLS model is 93.56%. However, it partitioned

**Table 1** Overlapping area error metrics of the segmentation of clinical BUS images

| Methods | TP ratio (%) | FP ratio (%) | FN ratio (%) | SI ratio (%) |
|---|---|---|---|---|
| EBLS method | 95.74 | 34.97 | 4.26 | 70.93 |
| LSAC method | 92.32 | 19.23 | 7.68 | 80.33 |
| The proposed method | 93.56 | 8.10 | 6.44 | 87.12 |

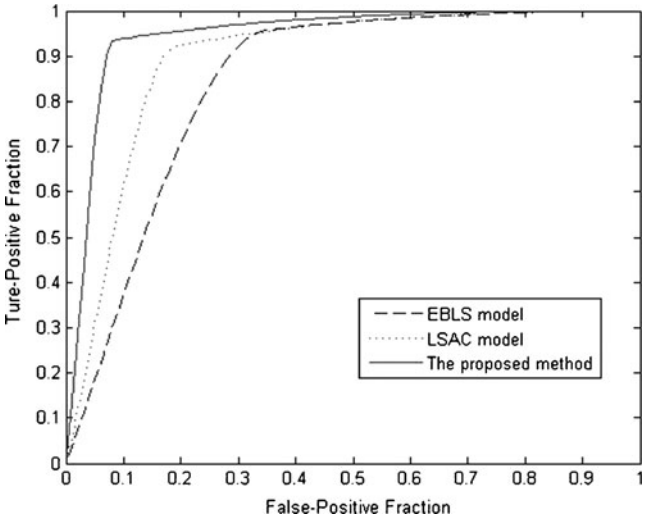


**Fig. 8** Statistical analysis of the ROC curve for evaluating the overall performance of the three methods

many normal tissues into the lesion region and the generated boundary exceeds the real lesion region greatly, causing the FP ratio to be as high as 34.97%. A high FP can cause more unnecessary biopsies or surgeries and will make the patients suffer from emotional pressure. In addition, due to the high FP ratio, its overall performance is quite poor (SI=70.93%). The LSAC model has a fairly good performance, with an SI ratio of 80.33%. However, the blurry boundaries cannot be handled well by only considering the gray levels since the gray levels around the boundaries between lesion and normal tissues are quite similar. Also, its FP ratio (19.23%) is quite high. Compared with the EBLS and the LSAC models, the proposed method obtained the best similarity (SI= 87.12%), much higher than that of the other two methods, i.e., its overall performance is the best. The statistical analysis of the ROC curve for evaluating the overall performance of the three methods is shown in Fig. 8. The AUCs of the proposed method, the LSAC model, and the EBLS model are 0.9525, 0.8999, and 0.8498, respectively. This demonstrates that the segmentation result of the proposed method is very accurate.

Table 2 is the statistical evaluation of the three methods using Hausdorff distance. In each column, the Hausdorff distances (mean (Mean*H*) and standard deviation (Std*H*)) between the 205 segmentation results and the corresponding manual delineations are presented. The Hausdorff distance of the proposed method is significantly lower than that of the other two methods and indicates that the proposed method is more reliable in segmenting BUS images.

The proposed method is also compared with the grow cut method. Since the grow cut is interactive, we cannot use the

**Table 2** Statistical evaluation with Hausdorff distance

| Method | Hausdorff distance between the results of the method and the radiologist | |
|---|---|---|
| | Mean*H* | Std*H* |
| EBLS method | 78.93 | 40.45 |
| LSAC method | 48.28 | 22.91 |
| Proposed method | 26.33 | 15.62 |

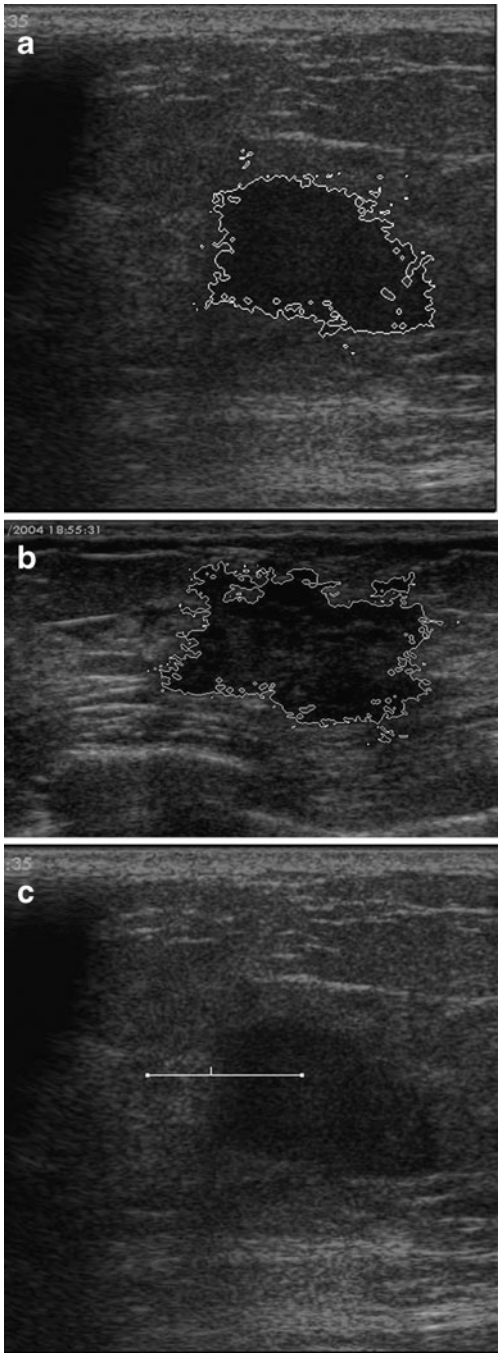


**Fig. 9** Segmentation result comparison between the proposed method and the grow cut method. **a** Segmentation result of Fig. 6a by the grow cut method. **b** Segmentation result of Fig. 7a by the grow cut method. **c** Converge position of the proposed method in Fig. 2b

statistical method to evaluate the performance. However, from Fig. 9a, b, we can see that the boundaries generated by grow cut with $K$=4 Moore neighborhood system are quite zigzag, and this may seriously affect feature extraction. It is observed from Figs. 6d and 7d, by utilizing the new neighborhood system, that the proposed method could generate smoother boundaries than by using the grow cut method. In the case of an inhomogeneous gray level (Fig. 2a), the grow cut method can converge on wrong positions. Utilizing the proposed method with the same initial condition, the convergent position of the dashed line in Fig. 2b is generated in Fig. 9c. Compared with the grow cut method, the position converged by the proposed method is much closer to the real lesion boundary. The experiments were implemented using a Core 4 PC with 4 GB RAM and an average process time of 35 s. The speed of the grow cut method using $K$=4 Moore neighborhood system is quite slower, which was more than 65 s. Moreover, the segmentation process of the proposed method is not interactive.

## Conclusion

In this paper, a novel method based on cellular automata is proposed for lesion segmentation within a BUS image. Different energy transfer strategies are developed and utilized for modeling the energy transition function. The proposed method is operated on a series of clinical BUS images for studying its characteristic and evaluating its performance; two other methods are also applied to the same images for comparison. In most of the images, due to serious speckle noise, there are blurry boundaries between different regions and the contrast is also low. In addition, the shapes of lesion regions are in great variations. The segmentation results of the proposed method with the results of the other two segmentation methods are compared with the manual delineations by an experienced radiologist. The overlapping area error metrics and statistical evaluations are utilized for evaluating the segmentation results, and the trade-off between TP versus FP of the three methods is also studied by ROC statistical analysis. The proposed method produces much better results than the other two methods. The experimental results show that the proposed method has the advantage in dealing with blurry boundaries, is robust to noise, and is insensitive to initial condition.

There are two issues which should be investigated in the future. Since the proposed method is a ROI segmentation-based method, the limitation of the proposed method is that the ROIs are generated by manual delineations. In future research, the ROIs should be produced automatically. The second one is that we use the delineations of a single expert as the gold standard. In future work, we would like to involve more experienced radiologists. The proposed approach may find wide application in BUS imaging and CAD systems.

**Acknowledgment** Financial support from the National Nature Science Foundation of China (NSFC) and Outstanding Academic Researchers Project of Harbin Science and Technology Bureau is greatly appreciated (grant nos. 60873142, 61100097, and 2009RFXXS211).

## References

1. Jemal A, Siegel R, Ward E, Hao Y, Xu J, Murray T: Cancer statistics, 2008. Cancer J Clin 58:71–96, 2008
2. Cheng HD, Shi X, Min R, Hu L, Cai X, Du H: Approaches for automated detection and classification of masses in mammograms. Pattern Recognition 39(4):646–668, 2006
3. Cheng HD, Shan J, Ju W, Guo YH, Zhang L: Automated breast cancer detection and classification using ultrasound images: a survey. Pattern Recognition 43:299–317, 2010
4. Cheng HD, Jiang XH, Sun Y, Wang JL: Color image segmentation: advances and prospects. Pattern Recognition 34(12):2259–2281, 2001
5. Horsch K, Giger ML, Venta LA, Vyborny CJ: Computerized diagnosis of breast lesions on ultrasound. Med Phys 29(2):157–164, 2002
6. Drukker K, Giger ML, Horsch K, Kupinski MA, Vyborny CJ, Mendelson EB: Computerized lesion detection on breast ultrasound. Med Phy 29(7):1438–1446, 2002
7. Madabhushi A, Metaxas DN: Combining low–high-level and empirical domain knowledge for automated segmentation of ultrasonic breast lesions. IEEE Trans Med Imag 22(2):155–169, 2003
8. Boukerroui D, Baskurt A, Noble JA, Basset O: Segmentation of ultrasound images—multiresolution 2D and 3D algorithm based on global and local statistics. Pattern Recogn Lett 24:779–790, 2003
9. Xiao GF, Brady M, Noble JA, Zhang YY: Segmentation of ultrasound B-mode images with intensity inhomogeneity correction. IEEE Trans Med Imag 21(1):48–57, 2002
10. Cheng HD, Hu L, Tian J, Sun L: A novel Markov random field segmentation algorithm and its application to breast ultrasound image analysis. The 6th International Conference on Computer Vision, Pattern Recognition and Image Processing, Salt Lake City, USA, p 159, 2005
11. Chen DR, Chang RF, Wu WJ, Moon WK, Wu WL: 3-D breast ultrasound segmentation using active contour model. Ultrasound Med Biol 29(7):1017–1026, 2003
12. Chang RF, Wu WJ, Moon WK, Chen WM, Lee W, Chen DR: Segmentation of breast tumor in three-dimensional ultrasound images using three-dimensional discrete active contour model. Ultrasound Med Biol 29(11):1571–1581, 2003
13. Chen DR, Chang RF, Kuo WJ, Chen MC, Huang YL: Diagnosis of breast tumors with sonographic texture analysis using wavelet transform and neural networks. Ultrasound Med Biol 28(10):1301–1310, 2002
14. Huang YL, Chen DR: Watershed segmentation for breast tumor in 2-D sonography. Ultrasound Med Biol 30:625–632, 2004
15. Chen CM, Chou YH, Chen CSK: Cell-competition: a new segmentation algorithm for multiple objects with irregular boundaries in ultrasound images. Ultrasound Med Biol 31(12):1647–1664, 2005
16. Chang RF, Wu WJ, Moon WK, Chen DR: Automatic ultrasound segmentation and morphology based diagnosis of solid breast tumors. Breast Cancer Res Treat 89(2):179–185, 2005
17. Liu B, Cheng HD, Huang JH, Tian JW, Liu JF, Tang XL: Automated segmentation of ultrasonic breast lesions using statistical texture classification and active contour based on probability distance. Ultrasound Med Biol 35(8):1309–1324, 2009

18. Liu B, Cheng HD, Huang JH, Tian JW, Tang XL, Liu JF: Probability density difference-based active contour for ultrasound image segmentation. Pattern Recognition 43:2028–2042, 2010
19. Chen Y, Yin RM, Flynn R, Broschat S: Aggressive region growing for speckle reduction in ultrasound images. Pattern Recognition lett 24:677–691, 2003
20. Michailovich OV, Tannenbaum A: Despeckling of medical ultrasound images. IEEE Trans Ultrason Ferroelectr Freq Control 53 (1):64–78, 2006
21. Noble JA, Boukerroui D: Ultrasound image segmentation: a survey. IEEE Trans Med Imag 25(8):987–1010, 2006
22. Radu V, Thomas C: Pattern generation using likelihood inference for cellular automata. IEEE Trans Imag Pro 15(7):1718–1727, 2006
23. Wang CY, Cheng L: Feature extracting of geographical image with status transfer of cellular automata. Proceedings of the International Symposium on Intelligent Information Systems and Applications, pp 307–309, 2009
24. Popovici A, Popovici D: Cellular automata in image processing. Fifteenth International Symposium on Mathematical Theory of Networks and Systems, pp 34–44, 2000
25. Hernandez G, Herrmann HJ: Cellular automata for elementary image enhancement. CVGIP: Graphical Model and Image Processing 58(1):82–89, 1996
26. Vezhnevets V, Konouchine V: "Grow cut"—interactive multi-label N-D image segmentation by cellular automata. Proceedings of Graphicon, pp 150–156, 2005
27. Sun YF, Chen Yan, Zhang YZ: Automated seeded region growing method for document image binarization based on topographic features. Image Analysis and Recognition, pp 200–208, 2004
28. Weszka J, Dyer C, Rosenfeld A: A comparative study of texture measures for terrain classification. IEEE Trans Syst Man Cybern 6 (4):269–285, 1976
29. Haralick RM, Shanmugam HK, Dinstein I: Texture parameters for image classification. IEEE Trans Syst Man Cybern 3(6):610–621, 1973
30. Gordon R, Rangayyan RM: Feature enhancement of film mammograms using fixed and adaptive neighborhoods. Appl Opt 23 (4):560–564, 1984
31. Kevin W, Kevin WB: Generating ROC curves for artificial neural networks. IEEE Trans Med Imag 16(3):329–336, 1997
32. Perona J, Malik J: Scale-space and edge-detection using anisotropic diffusion. IEEE Trans Pattern Anal Mach Intell 12(7):629–639, 1990
33. Czerwinski RN, Jones DL, O'Brien WD: Detection of lines and boundaries in speckle images—application to medical ultrasound. IEEE Trans Med Imag 18(2):126–136, 1999